

¹ Chapter 1

² Signal formation in diamond

³ This chapter describes the fundamentals of signal formation in a diamond sensor,
⁴ as well as its use as a particle detector. This is described in section 1.1 where the
⁵ principles of energy deposition are explained. Then the current signal shapes of
⁶ different types of radiation are shown. Later on the internal lattice defects that affect
⁷ the signal are described. The final section contains the description of the remaining
⁸ part of the signal chain – signal amplifiers, digitisers and devices for signal processing.
⁹ Noise contributions are discussed at every stage of the signal chain.

¹⁰ Ionisation is the main signal generation mechanism in diamond, silicon and other
¹¹ semiconducting materials. A semiconductor sensor converts the energy deposited
¹² by an incident energetic particle to an electrical signal. In particular, the particle
¹³ ionises the atoms in the lattice, freeing electrons and holes, which then drift towards
¹⁴ positively and negatively charged electrodes due to an externally applied electrical
¹⁵ field, inducing an electrical signal on the electrodes.

¹⁶ Silicon is currently considered as the industry standard for particle detection.
¹⁷ However, there are several disadvantages of using silicon instead of diamond, due
¹⁸ to significant differences in the material properties. In particular, the properties of
¹⁹ silicon change significantly with radiation. Due to radiation-induced lattice defects,
²⁰ which act as charge traps, the charge collection efficiency is decreased. The defects
²¹ are also responsible for the increase of the leakage current, increasing the shot noise
²² eventually leading to a thermal runaway. The same is true for diamond, but on a
²³ smaller scale.

²⁴ Table 1.1 compares the properties of diamond and silicon. Some of these values
²⁵ are revisited and used in the course of this thesis.

1.1. PRINCIPLES OF SIGNAL FORMATION IN SEMICONDUCTORS

Property	Diamond	Silicon
Band gap energy E_g (eV)	5.5	1.12
Electron mobility μ_e ($\text{cm}^2 \text{ V}^{-1} \text{ s}^{-1}$)	1800	1350
Hole mobility μ_h ($\text{cm}^2 \text{ V}^{-1} \text{ s}^{-1}$)	1200	450
Breakdown field (V cm^{-1})	10^7	3×10^5
Resistivity ($\Omega \text{ cm}$)	$> 10^{11}$	2.3×10^5
Intrinsic carrier density (cm^{-3})	$< 10^3$	1.5×10^{10}
Mass density (g cm^{-3})	3.52	2.33
Atomic charge	6	14
Dielectric constant ϵ	5.7	11.9
Displacement energy (eV/atom)	43	13 – 20
Energy to create an e-h pair (eV)	13	3.6
Radiation length (cm)	12.2	9.6
Avg. signal created/ μm (e)	36	89

Table 1.1: Comparison diamond – silicon [?, ?].

1.1 Principles of signal formation in semiconductors

Particles can interact with the sensor in several ways, e.g. via bremsstrahlung [], elastic or inelastic scattering (e-h pair production) or nuclear reactions. Bremsstrahlung is radiation created when a particle is decelerated due to interaction with the electric field of the core of an atom. Elastic scattering is deflection of the particle's trajectory due to the pull from the nucleus without depositing any energy in it. This is in principle an unwanted effect in semiconductors as it deteriorates the spatial resolution of the sensor. Inelastic scattering is the interaction through which an atom is ionised and an electron-hole pair is created. All these effects are competing and are dependent on the particle's mass, momentum etc.

Semiconductors are materials with a conductance between that of insulators and that of metals – of the order of $10^{?5} \Omega^{-1} \text{ cm}^{?1}$. They can be made up of atoms with four electrons in their valence band (e.g. silicon–Si, carbon–C or germanium–Ge) or as combinations of two or more different materials (e.g. gallium arsenide–GaAs). The atoms in the lattice form valence bonds with adjacent atoms, making solid crystal structures.

The valence bonds between atoms in the crystal lattice can break apart if sufficient external energy is deposited. The electron that was forming the bond is excited into the conductance band, leaving behind a positively charged ion with a vacancy – a hole – in its valence band, as shown in figure 1.1a. A free electron-hole pair is thus created. The free electron travels through the crystal until it is recombined with another hole. Similarly, the hole also travels through the material. Its positive charge attracts a bound electron in the vicinity, which breaks from the current bond and moves to the vacancy, leaving a new hole behind. The process continues, making it look like the hole is traveling through the material [].

The electrons need to absorb a certain energy to get to get ionised. The minimal

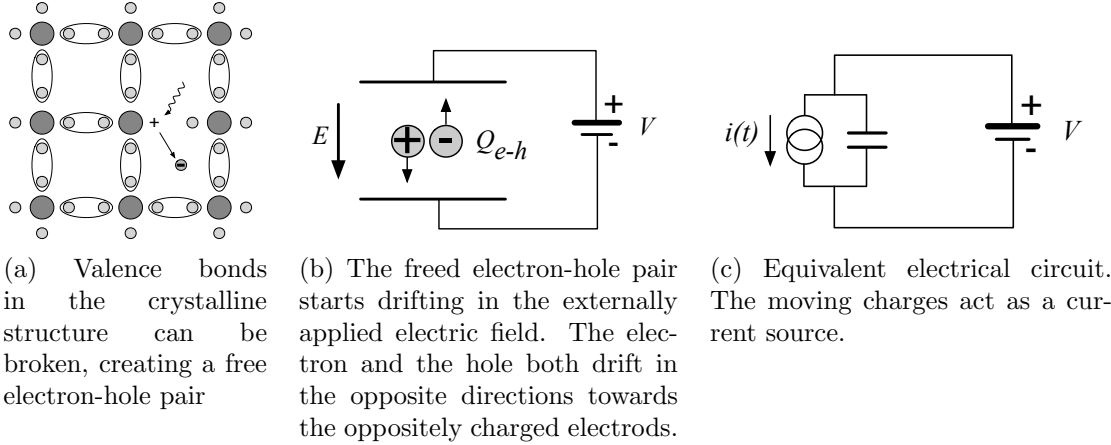


Figure 1.1: In the equivalent electrical circuit diagram the electron-hole creation and drift can be modelled as a current source with a capacitor in parallel.

transferred energy required to excite an electron in a semiconductor is equal to the energy gap E_g . Typical widths of the forbidden gap are 0.7 eV in Ge, 1.12 eV in Si, 1.4 eV in GaAs and 5.5 eV in diamond. Due to the small band gap in semiconductors a significant amount of electrons already occupies the conduction band at room temperature (RT) due to thermal excitation, according to the probabilistic distribution. The intrinsic carrier concentration n_i in semiconductors is given as

$$n_i = T^{3/2} \cdot \exp\left(-\frac{E_g}{2k_B T}\right) \quad (1.1)$$

wherein $k_B = 1.381 \times 10^{-23} \text{ m}^2 \text{ kg s}^{-2} \text{ K}^{-1}$ is the Boltzmann constant, E_g is the energy band gap of the semiconductor and T is the temperature in K.

If an external electric field is applied to the crystalline structure, the free electrons and holes drift toward the positive and negative potential, respectively, as shown in figure 1.1b. While drifting, the charges couple with the electrodes, inducing current in the circuit, which is explained by the Shockley–Ramo theorem below. Upon reaching the electrodes the charges stop inducing the current. The equivalent electrical circuit is shown in figure 1.1c.

Mean energy loss of a particle traversing the detector as a function of the momentum is given with the the Bethe-Bloch equation []:

$$-\left\langle \frac{dE}{dx} \right\rangle = \frac{4\pi}{m_e c^2} \cdot \frac{n z^2}{\beta^2} \cdot \left(\frac{e^2}{4\pi\epsilon_0} \right)^2 \cdot \left(\ln \left(\frac{2m_e c^2 \beta^2}{I \cdot (1 - \beta^2)} \right) - \beta^2 \right) \quad (1.2)$$

The resulting function for a muon is shown in figure 1.2. At a momentum of around 300 MeV/c the particle deposits the lowest amount of energy. That is called a minimum ionising particle or a MIP.

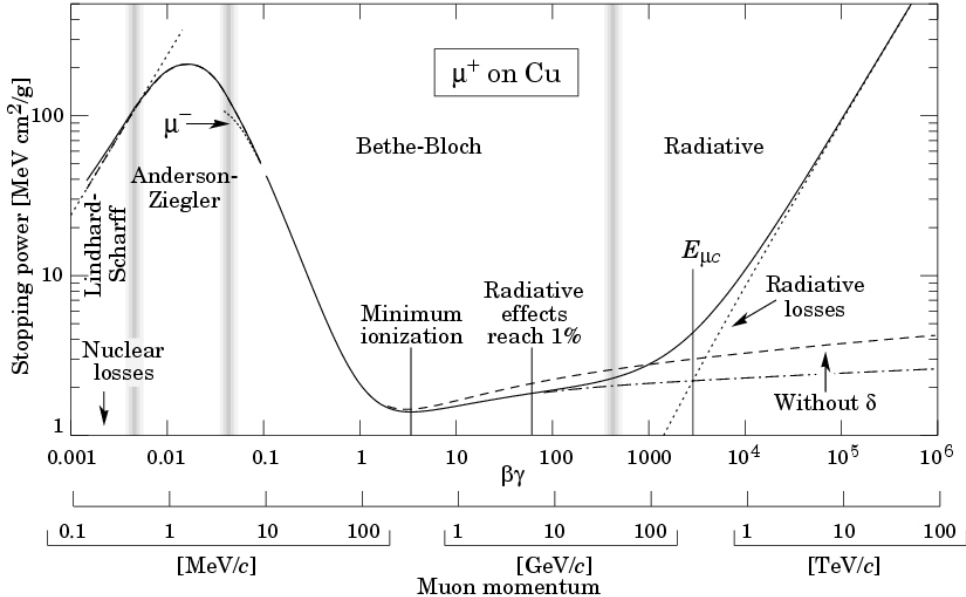


Figure 1.2: Stopping power for muons according to the Bethe-Bloch formula [].

⁷⁴ 1.1.1 Signal induction by moving charges

⁷⁵ The signal induction in a conducting plane by a point-like charge, which couples with
⁷⁶ an electrode, is derived in [2]. The electrode can in this case be modelled as an infinite
⁷⁷ conducting plane. When a point charge q is created (e.g. an electron-hole pair created
⁷⁸ via ionisation), its electrostatic field lines immediately couple with the electrode, as
⁷⁹ seen in figure 1.3a. The electric field on the metal surface due to a point-like charge
⁸⁰ q at the distance z_0 is

$$E_z(x, y) = \frac{q z_0}{2\pi\epsilon_0(x^2 + y^2 + z_0^2)^{\frac{3}{2}}} \quad E_y = E_z = 0. \quad (1.3)$$

⁸¹ A mirror charge appears on the conducting plane, with a charge density distribution

$$\sigma(x, y) = \epsilon_0 E_z(x, y) = \frac{q z_0}{2\pi(x^2 + y^2 + z_0^2)^{\frac{3}{2}}}. \quad (1.4)$$

⁸² The charge density integrated over the entire plane yields a mirror charge Q , which
⁸³ is an opposite of point charge q :

$$Q = \int_{-\infty}^{\infty} \int_{-\infty}^{\infty} \sigma(x, y) dx dy = -q. \quad (1.5)$$

⁸⁴ The plane is then segmented into infinitely long strips with a width w whereby each
⁸⁵ of the strips is grounded, as shown in figure 1.3c. Considering a charge density
⁸⁶ distribution 1.4, the resulting mirror charge on a single strip Q_2 directly below the
⁸⁷ point charge ($x = 0, y = 0$) yields

$$Q_2(z_0) = \int_{-\infty}^{\infty} \int_{-w/2}^{w/2} \sigma(x, y) dx dy = -\frac{2q}{\pi} \arctan\left(\frac{w}{2z_0}\right) \quad (1.6)$$

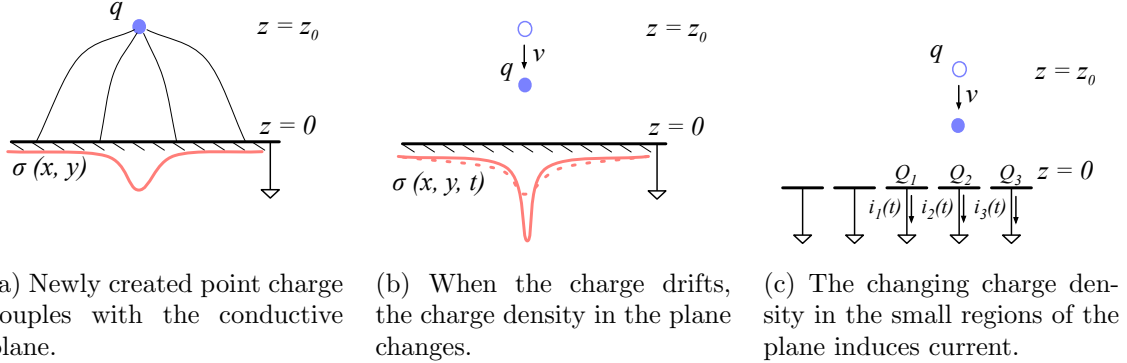


Figure 1.3: A point-like charge inducing current in a conductive plane.

If the charge starts moving towards the conducting plane, the mirror charge density distribution also changes, as shown in figure 1.3b. As a result the $Q_2[z(t)]$ changes with time. The changing charge is in effect an induced electric current $i_2(t)$:

$$i_2(t) = -\frac{d}{dt}Q_2[z(t)] = -\frac{\partial Q_2[z(t)]}{\partial z}\frac{\partial z(t)}{\partial t} = \frac{4qw}{\pi[4z(t)^2 + w^2]}v. \quad (1.7)$$

The movement of the point-like charge therefore induces current in the conducting plane. The induced current is linearly dependent on the velocity of the point-like charge.

1.1.2 Shockley-Ramo theorem

W. Shockley [6] and S. Ramo [5] independently proposed a theory which explains how a moving point charge induces current in a conductor. The Shockley-Ramo theorem can therefore be used to calculate the instantaneous electric current induced by the charge carrier or a group of charge carriers. It can be used for any number of electrodes. It states that the current $I_n^{\text{ind}}(t)$ induced on the grounded electrode n by a point charge q moving along a trajectory $\mathbf{x}(t)$ reads

$$I_n^{\text{ind}}(t) = -\frac{dQ_n(t)}{dt} = -\frac{q}{V_w}\nabla\Psi_n[\mathbf{x}(t)]v(t) = -\frac{q}{V_w}\mathbf{E}_n[\mathbf{x}(t)]v(t), \quad (1.8)$$

where $\mathbf{E}_n(\mathbf{x})$ is the *weighting field* of electrode n in the case where the charge q is removed, electrode n is set to voltage $V_w = 1$ and all other electrodes are grounded. The weighting field is defined as the spatial differential of the *weighting potential*: $\mathbf{E}_n(\mathbf{x}) = \nabla\Psi_n(\mathbf{x})$. In the case of two parallel electrodes, the weighting field is $E_w = -\frac{d\Psi}{dx} = -1/d$, where d is the distance between the electrodes. The resulting induced current is therefore

$$i(t) = \frac{q}{d}v_{\text{drift}}(x, t), \quad (1.9)$$

whereby v_{drift} is the drift velocity of the point-like charge and d is the distance between the electrodes.

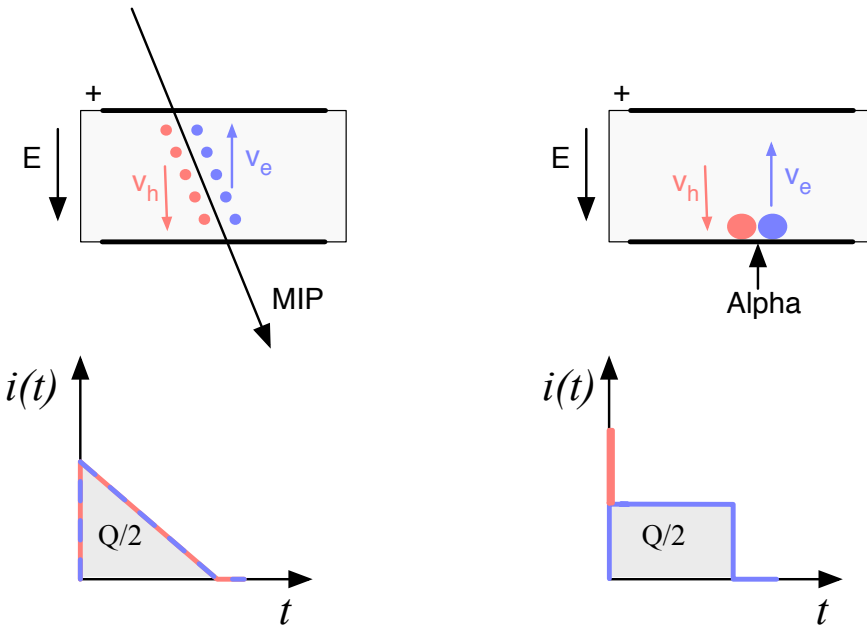


Figure 1.4: Charge carrier drift in diamond for β/γ and for α particles crossing the sensor at $t = 0$.

¹⁰⁹ 1.1.3 Radiation-induced electrical pulses

¹¹⁰ When a highly-energetic particle travels through the sensor, it interacts with atoms
¹¹¹ in the lattice. It ionises the valence electrons, creating electron-hole (e-h) pairs on
¹¹² its way. It can either deposit only a fraction of its energy and exit the sensor on the
¹¹³ other side or it can get stopped in the bulk, depositing all of its energy. A special
¹¹⁴ case is when it interacts with the core of the atom in the middle of the sensor via
¹¹⁵ a nuclear interaction. All these various types interactions produce different amounts
¹¹⁶ and different spatial distributions of e-h pairs. The induced electrical current there-
¹¹⁷ fore differs for different types of interaction. Two most frequent types are shown in
¹¹⁸ figure 1.4. The first diagram shows the interaction of a minimum ionising particle.
¹¹⁹ The electrons and holes are created all along the trajectory of the particle and imme-
¹²⁰ diately start drifting towards the positive and negative electrode, respectively. At the
¹²¹ beginning, all charges drift and contribute to the induced current. Those closest to
¹²² the electrodes have a very short drift path, reducing the induced current. Gradually
¹²³ all the charge carriers reach the electrode. The resulting current signal is a triangu-
¹²⁴ lar pulse with a sharp rising edge and a linear falling edge. The accumulated charge Q_s
¹²⁵ equals to the sum of the contributions of the positive and negative charge carriers.
¹²⁶ The second type of interaction happens when the particle is stopped in the diamond
¹²⁷ close to the point of entry. Most of its energy is deposited in a small volume close to
¹²⁸ the electrode. A cloud of charge carriers is created and the charges with the shorter
¹²⁹ path to the electrode disappear almost instantly. The carriers of the opposite charge,

however, start drifting through the sensor to the other electrode. In an ideal diamond sensor, their velocity is constant throughout the drift up until they are collected at the opposite electrode. The contribution of the first charge cloud is a peak with a short time. The cloud drifting through the sensor, on the other hand, induces a current signal with a flat top. The resulting signal has a shape of a rectangle, with a spike in the beginning. The accumulated charge Q_s is equal to a half of the deposited charge by the stopped particle.

The two aforementioned types of interactions have well defined signal responses. Nuclear interactions on the other hand yield various results. The resulting signal shape depends on the decay products of the interaction, which can be α , β or γ quanta or other nuclei, inducing a mixed shaped signal.

1.1.4 Signal charge fluctuations

Two important sensor properties are the magnitude of the signal and the fluctuations of the signal at a given absorbed energy. They determine the relative resolution $\Delta E/E$. For semiconductors the signal fluctuations are smaller than the simple statistical standard deviation $\sigma_Q = \sqrt{N_Q}$. Here N_Q is the number of released charge pairs, i.e. the ratio between the total deposited energy E_0 and the average energy deposition E_i required to produce an electron-hole pair. [] shows that the standard deviation is $\sigma_Q = \sqrt{FN_Q}$, where F is the Fano factor [] (0.08 for diamond and 0.115 for silicon []). Thus, the standard deviation of the signal charge is smaller than expected, $\sigma_Q \approx 0.3\sqrt{N_Q}$. The resulting intrinsic resolution of semiconductor detectors is

$$\Delta E_{\text{FWHM}} = 2.35\sqrt{FEE_i} \quad (1.10)$$

wherein $E_i(Si) = 3.6$ eV and $E_i(C) = 13$ eV. E.g., for an α particle with energy $E_\alpha = 5.486$ MeV the calculated resolution in diamond is equal to $\Delta E_{\text{FWHM}} = 5.6$ keV. This defines the minimum achievable resolution for energy spectroscopy with semiconductors. Figure 1.5 shows the resolution limit as a function of energy in silicon and diamond.

1.2 Carrier transport in a diamond sensor

This section describes the carrier transport phenomena in diamond. This theory provides the basis for discussion about the measurements in chapter ??.

When the charge carriers are freed in a semiconductor with no concentration gradient and without an externally applied electric field, they scatter in random directions with a thermal velocity v_{th} []. Their integral movement due to thermal excitation equals zero.

Diffusion Diffusion is caused by the concentration gradient. In its presence the integral movement is in the direction of the lower concentration until an equilibrium is

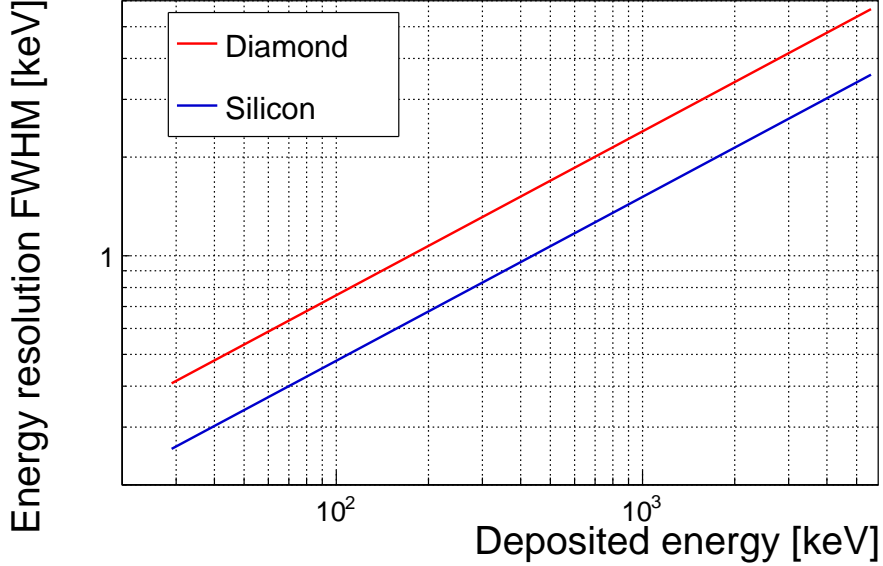


Figure 1.5: Calculated intrinsic energy resolution for silicon and diamond.

reached. The concentration profile dissolves with time forming a Gaussian distribution with variance $\sigma(t) = \sqrt{Dt}$ [] .

Drift Drift is caused by an externally applied electrical field. In that case the carriers move along the field lines. In a sensor with a high applied field the diffusion contribution is negligible.

Drift velocity, saturation velocity and mobility The charge carriers drift through the diamond bulk with a drift velocity $v_{\text{drift}}(E)$ [], which is proportional to the electric field E at low electric fields: $v_{\text{drift}} = \mu E$. The proportionality factor μ is defined as the mobility in $\text{cm}^2\text{V}^{-1}\text{s}^{-1}$.

For higher fields and higher velocities, however, the carriers lose more energy to the lattice. They induce increasingly more lattice vibrations (phonon transport). There is a velocity limit above which the carriers cannot reach – velocity saturation. The $v_{\text{sat}}^e = v_{\text{sat}}^h = (14.23 \pm 0.12) \times 10^6 \text{ cm/s}$ for both positive and negative charge carriers has been derived from the measurements in [4].

The final equation for v_{drift} is therefore

$$v_{\text{drift}}(E) = \mu(E)E = \frac{\mu_0 E}{1 + \frac{\mu_0 E}{v_{\text{sat}}}} \quad (1.11)$$

where μ_0 is the low field mobility and v_{sat} is saturation velocity. The drift velocity can be retrieved experimentally via the transit time measured with the Transient Current Technique (TCT). This technique enables the measurement of transit time t_t of the

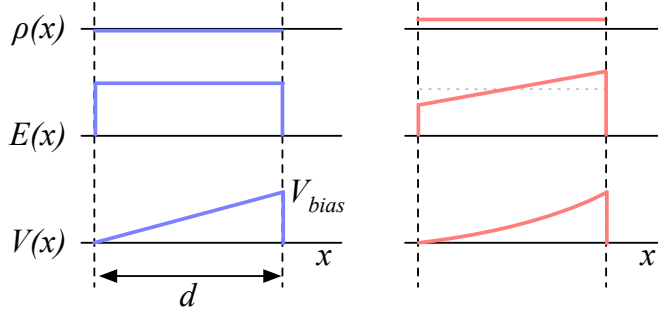


Figure 1.6: Left figure shows a profile of a diamond sensor only with an externally applied electric field. In the figure on the right a uniformly distributed space charge is added in the diamond, contributing to the internal electric field distribution. The induced current signal is proportional to the electrical field. d is the thickness of the diamond sensor.

¹⁸⁴ carriers through the sensor with the thickness d .

$$v_{\text{drift}}(E) = \frac{d}{t_t(E)}. \quad (1.12)$$

¹⁸⁵ The velocities for holes and electrons usually differ. In diamond, the holes travel
¹⁸⁶ 30 % faster than electrons []. The measurements in chapter ?? empirically confirm
¹⁸⁷ this statement.

¹⁸⁸ **Space charge** The Poisson equation shows that

$$\frac{d^2\Phi(x)}{dx^2} = \frac{dE(x)}{dx} = \frac{\rho(x)}{\epsilon} \quad (1.13)$$

¹⁸⁹ where $\rho(x)$ is the space charge distribution, E is the electrical field and Φ is the
¹⁹⁰ voltage potential. In an ideal diamond, the externally applied high voltage potential
¹⁹¹ on the two electrodes decreases linearly through the bulk. The electrical field is
¹⁹² therefore constant throughout the sensor and the space charge distribution across it
¹⁹³ equals 0. However, space charge may be introduced in the bulk either by means of
¹⁹⁴ accumulating of charge carriers in the lattice (i.e. charge trapping) or already during
¹⁹⁵ sensor production. The space charge can be either permanent or changing – sometimes
¹⁹⁶ it is possible to reduce it, as is shown in chapter ?. All in all, it is very important to
¹⁹⁷ reduce it because it affects the shape of the electrical signal. Since the drift velocity
¹⁹⁸ of the charge carriers is proportional to the electrical field, the charges change their
¹⁹⁹ velocity while drifting through the space charge region. Figure 1.6 compares the
²⁰⁰ voltage potential, the electrical field and the space charge for an ideal sensor as well
²⁰¹ as for that with a uniformly distributed positive space charge.

²⁰² **Radiation damage** The bonds in the diamond lattice are very strong. However,
²⁰³ when highly energetic particles hit the diamond, they can damage the crystal struc-
²⁰⁴ ture. Figure 1.7 shows several examples of lattice damage:

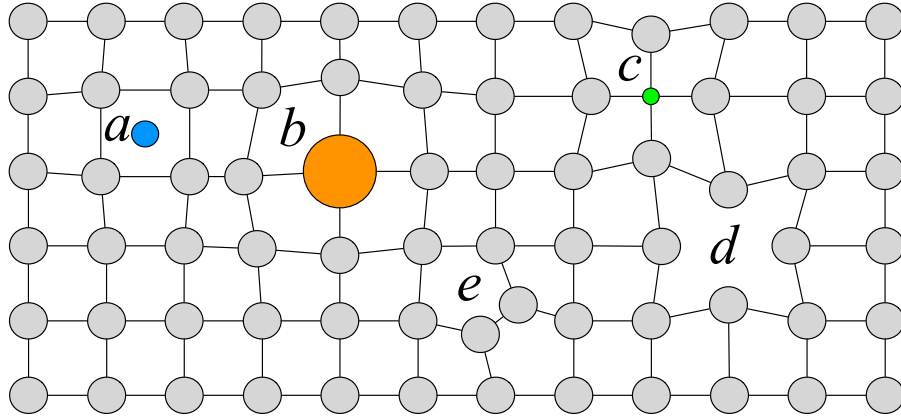


Figure 1.7: Impurities and non-uniformities in the crystal lattice due to radiation damage.

- 205 a) foreign interstitial (e.g. H, Li),
- 206 b, c) foreign substitutional (e.g. N, P, B),
- 207 d) vacancy and
- 208 e) self interstitial.

209 These non-uniformities form new energy levels in the forbidden gap – the separation
210 between the conductive and valence band in which the electrons. These intermediate
211 levels are referred to as charge traps because they can trap moving charge carriers.
212 The energy level of the trapped carriers is reduced from the conduction band to
213 the energy level of the trap. Different types of lattice damage have different energy
214 levels. The carriers trapped in an energy level close to the conduction band have a
215 high probability of being thermally excited back into the conduction band whereby
216 they continue drifting towards the electrode. Their activation energy is therefore low.
217 Those trapped in a deep trap close to the middle of the forbidden gap need a much
218 higher activation energy, which in turn increases the average time to their release due
219 to thermal excitation.

220 The trapped carriers do not contribute to the overall induced current on the elec-
221 trodes. The more charges are trapped along their drift path, the lower current is
222 induced on the electrodes.

223 1.3 Electronics for signal processing

224 This section describes the electronics of a detector, starting with a description of
225 signal amplifiers and then discussing the digitisation and signal processing. All these
226 stages are necessary to extract information from the sensor. First, the signal has to be

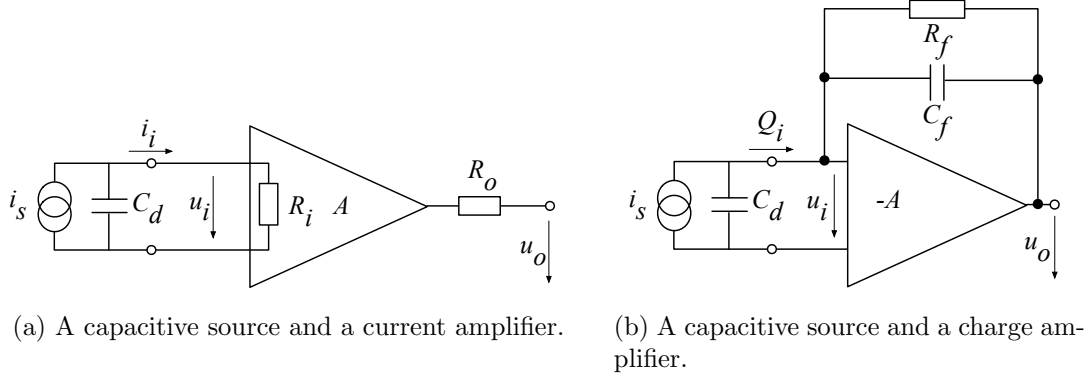


Figure 1.8: Simplified equivalent circuits of a current and charge amplifier.

amplified. Then it is digitised and finally processed in a specially designed processor or a logic unit.

1.3.1 Signal preamplifiers

The signal charge generated in the sensor by a single energetic particle is of the order of fC. The induced current range is typically between 10^{-8} A (β, γ radiation) and 3×10^{-7} A (α radiation). Signals as low as these have to be pre-amplified before processing. Depending on the measurement, several types of signal amplifiers can be used. The preamplifiers are designed to minimise electronic noise while maximising gain, thus maximising the signal-to-noise ratio (SNR). In addition, a high bandwidth limit is preferred to minimise the information loss due to signal shape deformation. A critical parameter is the total capacitance, i.e. the sensor capacitance together with the input capacitance of the preamplifier. The SNR improves with a lower capacitance. Several types of amplifiers can be used, all of which affect the measured pulse shape. Two preamplifiers are used most commonly, a current and a charge sensitive amplifier. Both are described in detail below.

Current-sensitive amplifier

Figure 1.8a shows the equivalent circuit of a capacitive source and a current amplifier. An amplifier operates in current mode if the source has a low charge collection time t_c with respect to the $R_i C_d$ time constant of the circuit. In this case the sensor capacitance discharges rapidly and the output current i_o is proportional to the instantaneous current i_i . The amplifier is providing a voltage gain, so the output signal voltage u_o is directly proportional to the input voltage u_i :

$$u_o(t) = A \cdot R_i \cdot i_s(t). \quad (1.14)$$

The detector capacitance C_{det} together with the input resistance of the amplifier R_i defines the time constant of the signal, as shown in figure 1.9. The higher the C_{det} ,

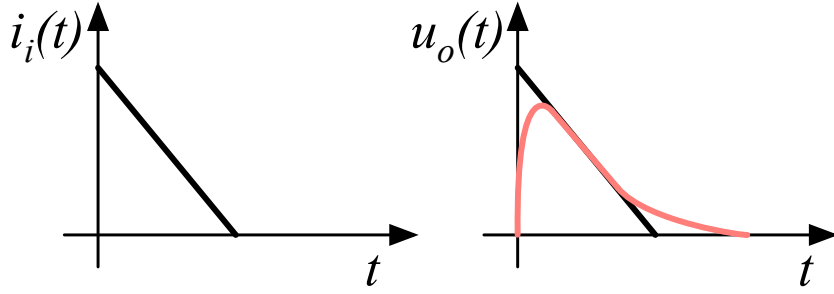


Figure 1.9: Input and output signal of the current amplifier.

251 the slower is the response of the amplifier. For the case of the diamond sensor, which
 252 has the capacitance of the order of 2 pF and the input resistance of 50Ω , the resulting
 253 time constant is $\tau = 10^{-10}$ s. This yields the signal rise time $t_r \sim 2.2\tau = 2.2 \times 10^{-10}$ s.
 254

255 Charge-sensitive amplifier

256 In order to measure integrated charge in the sensor, a feedback loop is added to the
 257 amplifier, as shown in figure 1.8b. The feedback can be used to control the gain and
 258 input resistance, as well as to integrate the input signal. The charge amplifier is in
 259 principle an inverting voltage amplifier with a high input resistance.

260 In an ideal amplifier the output voltage u_o equals $-Au_i$. Therefore the voltage
 261 difference across the capacitor C_f is $u_f = (A + 1)u_i$ and the charge deposited on the
 262 capacitor is $Q_f = C_f u_f = C_f(A + 1)u_i$. Since no current can flow into the amplifier,
 263 all of the signal current must charge up the feedback capacitance, so $Q_f = Q_i$.

264 In reality, however, charge-sensitive amplifiers respond much slower than is the
 265 duration of the current pulse from the sensor. In addition, a resistor is added to the
 266 feedback line in parallel to the capacitor. The resistor and capacitor define the decay
 267 time constant of the pulse, as shown in figure 1.10. This is necessary to return the
 268 signal to its initial state to be ready for a new measurement.

269 Analogue electronic noise

270 The electronic noise determines the ability of a system to distinguish different signal
 271 levels. The analogue signal contains ample information about the type and energy
 272 of incident radiation, which can quickly be erased or altered if the signal properties
 273 change. Therefore the noise contributions to the signal must be well understood
 274 to qualify the information the signal is carrying. The important contributions are
 275 listed below. Thermal or Johnson–Nyquist [] noise is the dominant noise contribution
 276 in the use case for diamond detector signal amplification and therefore defines the
 277 limitations of the detector system. This noise type is generated by the random thermal

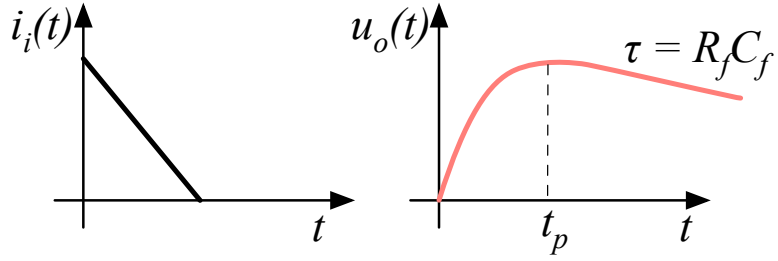


Figure 1.10: Input and output signal of the charge amplifier.

278 motion of charge carriers. The frequency range of the thermal noise is from 0 to ∞
279 with a predominantly uniform distribution. Therefore this is nearly a white noise.
280 The resulting signal amplitude has a Gaussian distribution. The RMS of the noise
281 amplitude is defined as

$$u_{\text{RMS}} = \sqrt{4k_B RT \Delta f} \quad (1.15)$$

282 where k_B is the Boltzmann constant, R is the input resistance of the amplifier, T its
283 temperature and Δf the frequency range. This equation shows that it is possible to
284 reduce the noise RMS by either (1) reducing the frequency range, (2) reducing the
285 resistance of the conductor or (3) cooling the conductor.

286 Contributions of shot noise, flicker noise and burst noise and other types are not
287 significant relative to the thermal noise. However, the contributions of external factors
288 can severely deteriorate the signal. This means the noise produced by capacitive or
289 inductive coupling with an external source, which causes interference in the signal.
290 These effects can be reduced by shielding the electronics and avoiding ground loops.

291 1.3.2 Analogue-to-digital converters

292 An analogue-to-digital converter (ADC) is a device that converts the analogue elec-
293 trical signal on the input to its digital representation - a series of digital values. This
294 involves a quantisation – *sampling* of the signal at a defined sampling period, resulting
295 in a sequence of samples at a discrete time period and with discrete amplitude values.
296 The resolution of the ADC is the number of output levels the ADC can quantise to
297 and is expressed in bits. For instance, an ADC with a resolution equal to $n = 8$ bit
298 has a dynamic range of $N = 2^n = 256$ steps. The resulting voltage resolution Q_{ADC}
299 at the input voltage range of $V_{\text{ADC}} = \pm 50$ mV is then

$$Q_{\text{ADC}} = \frac{V_{\text{ADC}}}{2^n} = \frac{100 \text{ mV}}{2^8 \text{ bit}} = 0.39 \text{ mV/bit.} \quad (1.16)$$

300 With a sampling period of $t_s = 1$ ns the sampling rate is $f_s = 1$ GS/s (gigasample per
301 second).

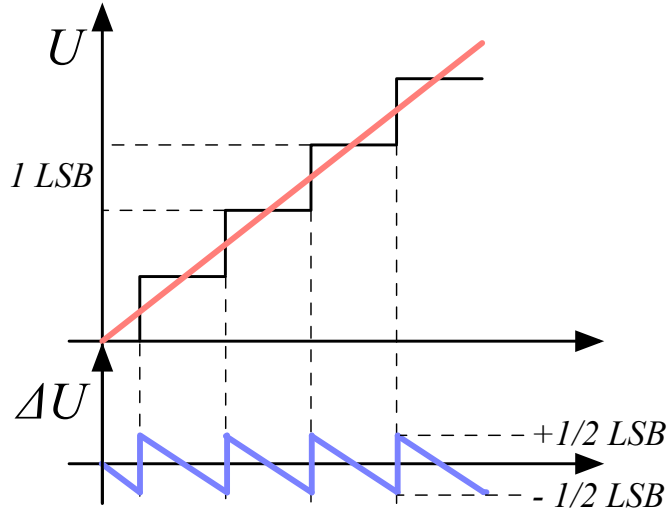


Figure 1.11: Input signal digitisation and quantisation error.

Quantisation error and quantisation noise (or a round-off error) is a contribution to the overall measurement error due to digitisation (rounding). The quantisation error is defined as a difference between the actual analog value and the closest digitised representation of this value, therefore by the least significant bit (LSB), as seen in figure 1.11. The input signal amplitude is typically much larger than the voltage resolution. In this case the quantisation error is not directly correlated with the signal and has an approximately uniform distribution \square . The probability density function $P(x)$ therefore has a rectangular shape bounded by $(-\frac{1}{2}\text{LSB}, \frac{1}{2}\text{LSB})$:

$$P(x) = \begin{cases} \frac{1}{\text{LSB}}, & -\frac{1}{2}\text{LSB} \leq x \leq \frac{1}{2}\text{LSB} \\ 0, & \text{otherwise.} \end{cases} \quad (1.17)$$

302 The height equal to $\frac{1}{\text{LSB}}$ preserves the integrated probability of 1. The variance of
303 the distribution is

$$\sigma^2 = \int P(x)(x - \mu)^2 dx. \quad (1.19)$$

304 The population mean is $\mu = 0$, therefore

$$\sigma^2 = \int_{-\frac{1}{2}\text{LSB}}^{\frac{1}{2}\text{LSB}} \frac{1}{\text{LSB}} x^2 dx = \frac{x^3}{3\text{LSB}} \Big|_{-\frac{1}{2}\text{LSB}}^{\frac{1}{2}\text{LSB}} = \frac{\text{LSB}^2}{12}. \quad (1.20)$$

305 The RMS of the quantisation noise is defined as the square root of the variance:

$$\Delta Q_{\text{ADC}} = \sqrt{\sigma^2} = \frac{1}{\sqrt{12}} \text{LSB} \sim 0.289 \text{ LSB}. \quad (1.21)$$

306 For the example above the quantisation error equals $\Delta Q_{\text{ADC}} = 0.289 \cdot 0.39 \text{ mV} =$
307 0.11 mV . The error depends strongly on the linearity of the ADC, but this is out of
308 scope of this document as the devices used have ADCs with a very good linearity.

309 **1.3.3 Digital signal processing**

310 The digitised signal can be processed to extract useful information. Therefore after
311 the signal amplification and digitisation the signal is routed in a device which handles
312 the digital analysis. The signal can either be processed immediately (in real time) or
313 it can be saved to a data storage for analysis at a later stage (offline). The devices
314 carrying out the processing can be multipurpose (e.g. Field Programmable Gate
315 Arrays) or dedicated (e.g. Application-Specific Integrated Circuits).

316 **Field Programmable Gate Array** (FPGA) is an integrated circuit designed to be
317 reprogrammable and reconfigured after manufacturing. It consists of a set of logic
318 gates that can be interconnected in numerous combinations to carry out a set of
319 logic operations. Many such logic operations can take place in parallel, making the
320 FPGA a powerful tool for signal processing. FPGAs are often used during system
321 development or in systems in which the requirements might change with time. They
322 can be reprogrammed in the order of seconds. In addition, the logic design only needs
323 minor changes when migrating to a newer version of the FPGA chip of the same
324 vendor. The FPGAs also offer faster time-to-market with comparison to application-
325 specific solutions, which have to be developed. On the other hand, the price per
326 part can be significantly higher than for the application-specific solutions. Also, their
327 other major disadvantages are a high power consumption and a relatively low speed
328 as compared to more application-specific solutions. However, today's solutions are
329 capable of clock speeds higher than 500 MHz. Together with the integrated digital
330 signal processing blocks, embedded processors and other modules, they are already
331 very powerful and versatile. All in all, FPGAs are a good choice for prototyping and
332 limited production, for projects with limited requirements for speed and complexity.

333 **Application-Specific Integrated Circuit** (ASIC) is an integrated circuit designed
334 for a specific use. The design cannot be modified after chip production, as is the case
335 with FPGAs. On the other hand, the ASICs can be optimised to perform a required
336 operation at a high speed and at a low power consumption. In addition, due to the
337 specific design the size of the chip can be much smaller. ASICs can be designed as
338 hybrid chips, containing both a digital and an analog part. Finally, ASICs can be
339 designed to withstand much higher irradiation doses than FPGAs and can therefore
340 be used in harsh environments like in space or in particle colliders.

341 To update the chip, the design has to be submitted to a foundry, which produces
342 the new chips with a turnover time of 4–6 weeks. The costs of a submission start
343 at \$ 50 000, but the price per part can be reduced significantly with a high volume.
344 To sum up, ASICs are used for high volume designs with well defined requirements

1.3. ELECTRONICS FOR SIGNAL PROCESSING

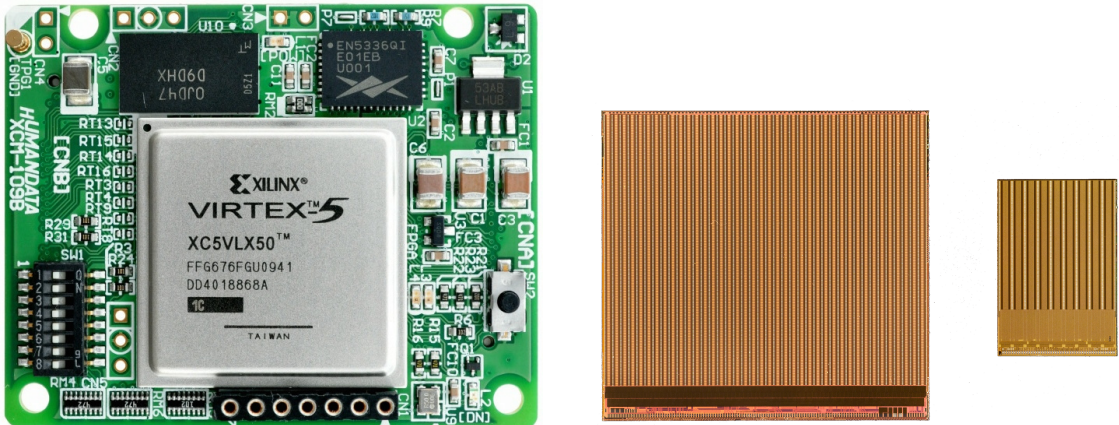


Figure 1.12: An example of a Xilinx Virtex 5 FPGA [1] and an FE-I4 and FE-I3 ASIC chip [3].

345 where some stringent constraints in terms of power consumption and speed have to
346 be met.

³⁴⁷ Bibliography

- ³⁴⁸ [1] *Xilinx Virtex 5 FPGA*. <http://www.hdl.co.jp/XCM-109/top.560.jpg>.
- ³⁴⁹ [2] W. Blum, W. Riegler, and L. Rolandi. Particle Detection with Drift Chambers,
³⁵⁰ volume 2 of 2. Springer-Verlag, Berlin Heidelberg, 2008.
- ³⁵¹ [3] M. Garcia-Sciveres. ATLAS Experiment Pixel Detector Upgrades. 2011.
- ³⁵² [4] Hendrik Jansen, Daniel Dobos, Thomas Eisel, Heinz Pernegger, Vladimir Eremin,
³⁵³ and Norbert Wermes. Temperature dependence of charge carrier mobility in
³⁵⁴ single-crystal chemical vapour deposition diamond. *Journal of Applied Physics*,
³⁵⁵ 113(17), 2013.
- ³⁵⁶ [5] S. Ramo. *Currents Induced by Electron Motion*. *Proceedings of the IRE*, 27:584–
³⁵⁷ 585, 1939.
- ³⁵⁸ [6] W. Shockley. *Currents to Conductors Induced by a Moving Point Charge*. *Journal*
³⁵⁹ *of applied Physics*, 9:635, 1938.